

# Surface plasmon resonance sensor utilizing an integrated organic light emitting diode

Jörg Frischeisen\*, Christian Mayr, Nils A. Reinke<sup>1</sup>, Stefan Nowy, Wolfgang Brütting\*

University of Augsburg, Institute of Physics, Universitätsstraße 1, 86159 Augsburg, Germany

<sup>1</sup> Present address: Institute for Computational Physics, Zürcher Hochschule der Angewandten Wissenschaften, PO Box 805, 8401 Winterthur, Switzerland

\*Corresponding authors: [joerg.frischeisen@physik.uni-augsburg.de](mailto:joerg.frischeisen@physik.uni-augsburg.de)  
[wolfgang.brueetting@physik.uni-augsburg.de](mailto:wolfgang.brueetting@physik.uni-augsburg.de)

**Abstract:** A novel surface plasmon resonance (SPR) sensor based on an integrated planar and polychromatic light source is presented. The sensor comprises an organic light emitting diode (OLED) and a metallic sensing layer located on opposite sides of a glass prism. We successfully fabricated and tested prototype sensors based on this approach by the use of different prism geometries and OLEDs with blue, green and red emission color. We investigated the angular and wavelength dependent SPR dispersion relation for sensing layers consisting of silver and gold in contact with air. Further on we demonstrated the sensor function by real time monitoring of temperature changes inside an adjacent water reservoir as well as by recording the dissolving process of sodium chloride in water. The presented technique offers the advantage that there is no necessity to couple light from external bulky sources such as lasers or halogen lamps into the sensing device which makes it particularly interesting for miniaturization.

©2008 Optical Society of America

**OCIS codes:** (130.6010) Sensors; (240.6680) Surface plasmons; (230.3670) Light-emitting diodes; (310.6860) Thin films, optical properties.

---

## References and links

1. J. Homola and S. S. Yee, "Surface plasmon resonance sensor based on planar light pipe: theoretical optimization analysis," *Sens. Actuators B* **37**, 145–150 (1996).
2. H. Raether, *Surface Plasmons on Smooth and Rough Surfaces and on Gratings* (Springer-Verlag, Berlin, 1988), Chap. 2.
3. S. A. Maier, *Plasmonics: Fundamentals and Applications* (Springer, Berlin, 2007), Chap. 2–3.
4. K. A. Peterlinz and R. Georgiadis, "Two-color approach for determination of thickness and dielectric constant of thin films using surface plasmon resonance spectroscopy," *Opt. Commun.* **130**, 260–266 (1996).
5. J. Homola, "Present and future of surface plasmon resonance biosensors," *Anal. Bioanal. Chem.* **377**, 528–539 (2003).
6. J. Homola, S. S. Yee, and G. Gauglitz, "Surface plasmon resonance sensors: review," *Sens. Actuators B* **54**, 3–15 (1999).
7. M. Leitz, A. Tamachkiarow, H. Franke, and K. T. V. Grattan, "Monitoring of biofilm growth using ATR-leaky mode spectroscopy," *J. Phys. D: Appl. Phys.* **35**, 55–60 (2002).
8. R. Ziblat, V. Lirtsman, D. Davidov, and B. Aroeti, "Infrared Surface Plasmon Resonance: A Novel Tool for Real Time Sensing of Variations in Living Cells," *Biophys. J.* **90**, 2592–2599 (2006).
9. V. Lirtsman, M. Golosovsky, and D. Davidov, "Infrared surface plasmon resonance technique for biological studies," *J. Appl. Phys.* **103**, 014702 (2008).
10. R. L. Rich and D. G. Myszka, "Advances in surface plasmon resonance biosensor analysis," *Curr. Opin. Biotechnol.* **11**, 54–61 (2000).
11. B. K. Singh and A. C. Hillier, "Surface Plasmon Resonance Imaging of Biomolecular Interactions on a Grating-Based Sensor Array," *Anal. Chem.* **78**, 2009–2018 (2006).
12. M. Manuel, B. Vidal, R. López, S. Alegret, J. Alonso-Chamarro, I. Garcés, and J. Mateo, "Determination of probable alcohol yield in musts by means of an SPR optical sensor," *Sens. Actuators B* **11**, 455–459 (1993).
13. M. W. Foster, D. J. Ferrell, and R. A. Lieberman, "Surface plasmon resonance biosensor miniaturization," *Proc. SPIE* **2293**, 122–131 (1994).
14. J. Melendez, R. Carr, D. U. Bartholomew, K. Kukanskis, J. Elkind, S. Yee, C. Furlong, and R. Woodbury, "A commercial solution for surface plasmon sensing," *Sens. Actuators B* **35–36**, 212–216 (1996).
15. H. P. Ho, S. Y. Wu, M. Yang, and A. C. Cheung, "Application of white light-emitting diode to surface plasmon resonance sensors," *Sens. Actuators B* **80**, 89–94 (2001).

16. L. Bürgi, R. Pfeiffer, M. Mücklich, P. Metzler, M. Kiy, and C. Winnewisser, "Optical proximity and touch sensors based on monolithically integrated polymer photodiodes and polymer LEDs," *Org. Electron.* **7**, 114–120 (2006).
  17. X. Wang, O. Hofmann, J. Huang, E. M. Barrett, R. Das, A. J. de Mello, J. C. de Mello, and D. D. C. Bradley, "Organic light emitting diodes and photodetectors: Toward applications in lab-on-a-chip portable devices," *Proc. SPIE* **6036**, 60361O (2005).
  18. P. Schiebener, J. Straub, J. M. H. Levelt Sengers, and J. S. Gallagher, "Refractive Index of Water and Steam as Function of Wavelength, Temperature and Density," *J. Phys. Chem. Ref. Data* **19**, 677–717 (1990).
  19. R. C. Weast (Ed.), *CRC Handbook of Chemistry and Physics*, 64th ed. (CRC Press, Inc., Boca Raton, 1983), pp. D-257–258.
  20. I. M. White and X. Fan, "On the performance quantification of resonant refractive index sensors," *Opt. Express* **16**, 1020–1028 (2008).
  21. R. Slavík and J. Homola, "Optical multilayers for LED-based surface plasmon resonance sensors," *Appl. Opt.* **45**, 3752–3759 (2006).
  22. S. R. Karlson, K. S. Johnston, S. S. Yee, and C. C. Jung, "First-order surface plasmon resonance sensor system based on a planar light pipe," *Sens. Actuators B* **32**, 137–141 (1996).
- 

## 1. Introduction

Surface plasmon resonance (SPR) sensors are based on electromagnetic surface plasmon waves (SPs) traveling at the interface between a dielectric and a metallic layer to detect changes of the refractive index of the dielectric close to the metal layer [1]. The excitation of surface plasmons is usually accomplished in the regime of attenuated total reflection when p-polarized light is incident on a metal-coated glass prism (Kretschmann's geometry) [2]. The SPR can be observed as a minimum of the reflectivity of the metal either as a function of the incidence angle or the wavelength. Thereby changes of the refractive index in the medium adjacent to the metal film can be detected by shifts of the SPR position [2,3]. Due to the extreme sensitivity to small variations in the refractive index of the probed medium, SPR sensors are ideally suited for a variety of applications including the non-invasive characterization of the optical constants and the thickness of thin films [4], monitoring of adsorption processes at metal surfaces [5], the real time and label-free analysis of biospecific interactions [6-8] or for the determination of the concentration of a material within a solvent [9].

In recent years there has been growing commercial interest in SPR sensors [5,10,11], especially through the development of compact devices. Miniaturized SPR sensors have been reported by several authors: Manuel and coworkers presented a robust SPR sensor based on a special prism coupling technique [12]. Foster and coworkers used a configuration which excites SPs by a convergent beam of monochromatic light [13]. However, the light source still remains a stumbling block in the development of small SPR sensors. Usually, SPR spectroscopy relies on bulky light sources with high power consumption, such as lasers or halogen lamps. There have been reports on the replacement of the traditional light sources by inorganic light emitting diodes (LEDs) [14,15]. A big drawback of these methods is that the fabrication of inorganic LEDs requires epitaxial techniques and crystalline substrates. Therefore, an additional molding step or coupling by optical components is necessary for the integration of inorganic LEDs into SPR sensors. This step limits the possibilities of miniaturization of the sensor device. Consequently, direct assembling of an integrated light source onto a monolithical SPR sensor device is desirable for the next step in sensor miniaturization.

In contrast to their inorganic counterparts, organic light emitting diodes (OLEDs) can be fabricated on almost any surface with an adequate smoothness as their growth does not require epitaxy. They are area emitters with a spectrally extended emission and are considered as promising candidates for general illumination and display technology. However, there have also been suggestions for other niche applications in recent years. Bürgi and coworkers developed an optical proximity and touch sensor based on monolithically integrated polymer light emitting diodes and polymer photodiodes [16]. Wang and coworkers reported that polymer light emitting diodes and polymer photodetectors can be integrated on disposable polydimethylsiloxane microfluidic flowcells [17].

In this work we demonstrate a novel SPR sensor on the basis of an integrated OLED light source. The sensor includes a metallic sensing layer and an organic light emitting diode located on opposite sides of one common prism. The light emitted by the OLED leaves the prism after reflection at the sensing layer. The spectral and angular dependent intensity of the reflected light for sensing layers consisting of silver and gold is analyzed. Further on, the sensor function is demonstrated by real time monitoring of temperature changes inside an adjacent water reservoir and by recording the dissolving process of sodium chloride (NaCl) in water.

## 2. Methodology

### 2.1 Fabrication of organic light emitting diodes and metallic sensing layers

Three OLEDs with different emission spectra were used as the SPR light source in our experiments. All OLEDs were fabricated on pre-cleaned commercial glass substrates covered with indium tin oxide (ITO) of 140 nm thickness (Merck Display Technologies, Type 859) as the anode. We deposited approximately 30 nm of the hole injection layer Poly(3,4-ethylenedioxythiophene) poly(styrenesulfonate) (PEDOT:PSS) by spin coating and all the other organic layers and metallic electrodes by thermal evaporation in a high vacuum system. The blue OLED comprises 40 nm of the hole transport material 2,2',7,7'-tetrakis-(N,N-diphenylamino)-9,9'-spirobifluoren (S-TAD), 30 nm of the blue emitter 4,4'-bis(2,2'-diphenylvinyl)-1,1'-spirobiphenyl (S-DPVBi), and 20 nm of the electron transporter Tris-(8-hydroxyquinoline) aluminum (Alq<sub>3</sub>). The green OLED consists of 80 nm S-TAD and 80 nm of the electron transporter and green emitter Alq<sub>3</sub>. Finally, the red OLED is made up of the same materials as the green OLED apart from a 20 nm wide zone of the Alq<sub>3</sub> layer at the interface to S-TAD being doped with the red dye 4-dicyanomethylene-2-methyl-6-(p-dimethylaminostyryl)-4H-pyran (DCM). The ratio of Alq<sub>3</sub>:DCM in the doped layer is 20:1 by weight. For the next 30 nm Alq<sub>3</sub> the deposition rate of DCM was linearly reduced to zero. All OLEDs had a 10 nm thick Ca layer covered by 120 to 150 nm Al as the cathode. Finally, we encapsulated the devices by a cover glass and UV-curing epoxy resin. As metallic sensor films, we thermally evaporated silver and gold on pre-cleaned glass substrates. For the measurements in aqueous environment, the metal sensing film was attached to a homemade glass cuvette so that about 14 ml solvent can be added.

### 2.2 Experimental setup

The experimental arrangement is shown in Fig. 1. For SPR measurements at the metal/air interface two right-angle prisms were connected by index matching gel to form one parallelogram and the OLED and the metallic sensing layer are attached to opposite sides of the prism by index matching gel, cf. Fig. 1(a).

For SPR measurements in aqueous environment the OLED is attached to the left edge of a trapezoidal plexiglass prism and the metallic sensing layer is located at the base of the prism with an angle of approximately 75 degrees between them, as shown in Fig. 1(b).

Inside the glass prism the OLED irradiates the metallic sensing layer with polychromatic light under various angles of incidence. The reflected light leaves through the edge of the prism and passes a linear polarizing filter so that only the p-polarized fraction is detected. A collimating lens focuses the light onto an optical fiber guiding it to a calibrated CCD spectrometer (Avantes AvaSpec-2048).

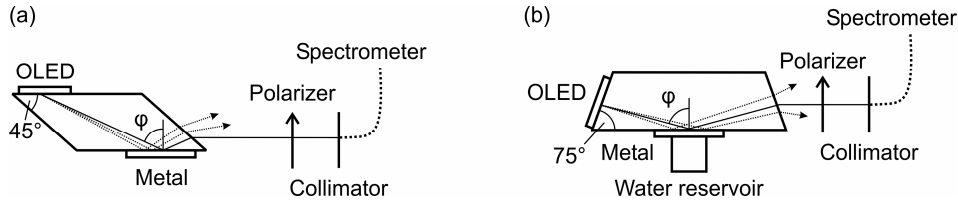


Fig. 1. Experimental setup: (a) for measurements in air an organic light emitting diode and a metallic sensor film are located on opposite sides of a glass prism which is mounted on a motorized rotation stage. The reflected light leaves through the edge of the prism and passes a linear polarizing filter before it is focused by a collimating lens onto an optical fiber guiding it to a spectrometer. (b) For measurements in aqueous environment the OLED and the metal film are attached to the edges of a trapezoidal plexiglass prism forming an angle of about 75 degrees towards the prism base.

For the measurement of the plasmon dispersion relation the prism was mounted on a motorized computer controlled rotation stage in such a way that the illuminated metal film was located on the axis of rotation. The angular dependence of the reflectivity of the metal film was detected by rotating the turntable in steps of 0.1 degree in the measurements with the red and green OLED and 0.2 degree for the blue OLED. A spectrum of the reflected light was recorded after each angle step. Additionally, the refraction of the light at the prism/air interface must be taken into account in order to determine the angle of incidence under which the light of the OLED impinges on the metal film.

In order to obtain the p-polarized reflectivity a reference measurement was performed for each experiment. Thereby the metallic sensor film was replaced by a glass substrate without a metallic layer and again a spectrum was recorded for each step. In the measured wavelength regime, total reflection occurs at the glass/air interface and the intensity of the reflected light is equal to the incident intensity. Hence by dividing the measured spectrum by the reference, one can obtain the p-polarized reflectivity for each angle. For the measurement over time in aqueous environment, which was performed at a fixed angle of incidence, the measured spectra were divided by one reference spectrum that was recorded under the same angle.

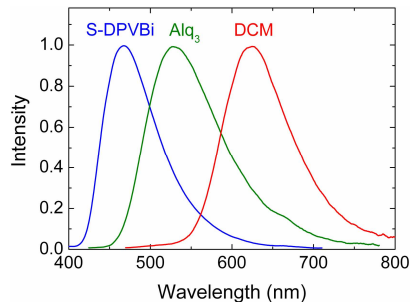


Fig. 2. OLED emission spectra normal to the substrate using three different organic emitters as described in the text.

Figure 2 shows the emission spectra of the blue, green and red OLEDs recorded in the normal direction towards the substrate plane. The full-width at half-maximum (FWHM) of the three OLEDs is about 20 % of the peak wavelength. The blue, green and red OLEDs have peak wavelengths of 465 nm, 530 nm and 625 nm, respectively, and cover almost the whole visible spectrum. The active area of all OLED pixels is 10 mm long and 0.5 mm wide, so that the OLED can be regarded as a linear light source. Compared to an OLED with a quadratic active area this geometry has the advantage that due to the small width all light originates from almost the same angular position while the large length increases the intensity of the detected light. A constant current source (Keithley, Type 220) drives the OLED with a current of 0.6 mA, corresponding to a moderate current density of 12 mA/cm<sup>2</sup>, so that there should be

no considerable degradation. If an OLED degrades over time the voltage required for a constant current usually increases. In our setup the voltage was monitored with a separate instrument (Keithley, Type 196) and no increase was observable. Hence the light output of the OLEDs can be assumed constant over time.

### 3. Results and discussion

#### 3.1 Metal/air interface

The following equation describes the dispersion relation for surface plasmons at the border of two half spaces [2]:

$$k_x = \frac{\omega}{c} \sqrt{\frac{\epsilon_1(\omega)\epsilon_2}{\epsilon_1(\omega) + \epsilon_2}}. \quad (1)$$

Therein  $k_x$  denotes the complex in-plane wave vector of the surface plasmon and  $\omega$  is the angular frequency of light.  $\epsilon_1(\omega) = \epsilon'_1(\omega) + i\epsilon''_1(\omega)$  denotes the complex dielectric function of the metallic sensing layer and  $\epsilon_2$  the dielectric constant of the environment. Using the fact that the in-plane wave vector is continuous across the glass/metal interface, i.e.  $k_x = (\omega/c) \cdot n_{\text{Substrate}} \cdot \sin \varphi$  with  $n_{\text{Substrate}}$  being the refractive index of the glass substrate, we find the following resonance condition for the incidence angle  $\varphi$  from the glass side:

$$\sin \varphi = \frac{1}{n_{\text{Substrate}}} \sqrt{\frac{\epsilon_1(\omega)\epsilon_2}{\epsilon_1(\omega) + \epsilon_2}} = \frac{1}{n_{\text{Substrate}}} \sqrt{\frac{\epsilon_1(\lambda)\epsilon_2}{\epsilon_1(\lambda) + \epsilon_2}}. \quad (2)$$

With this equation it is possible to determine the angle of resonant surface plasmon excitation for every wavelength  $\lambda$ . For instance one obtains a resonance angle of 43.8 degrees for a wavelength of 500 nm using optical constants of silver from ellipsometric measurements. Please note that this relation is strictly speaking only valid for semi-infinite metal films. For the usage as a sensor it is required to use metal films with a thickness of a few tens of nanometers so that the incident light can couple to SPs at the outer boundary of the metal film. In this case the metal thickness is finite and the resonance angle shifts slightly to higher angles. This behavior can be seen in Fig. 3 which shows the simulated p-polarized reflectivity at a wavelength of 500 nm for four different silver thicknesses. Thus Eq. (2) is not exactly valid for thin silver films but nevertheless can be used as a good approximation to determine the resonance angle.

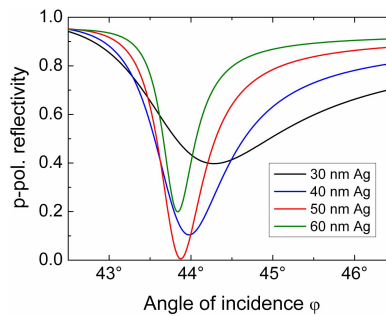


Fig. 3. Simulated p-polarized reflectivity of a glass/Ag/air interface for different silver thicknesses at a wavelength of 500 nm.

Besides the small influence on the angular position, the metal thickness strongly affects the magnitude of the light that couples to SPs traveling at the metal/air interface. For a wavelength of 500 nm the optimum thickness is between 48 and 50 nm. At this thickness,

maximum coupling to SPs occurs at an incidence angle of 43.9 degrees and the p-polarized reflectivity drops to virtually zero. Obviously, a more pronounced minimum results in a better signal-to-noise ratio. This illustrates the importance of choosing the optimum silver thickness, which depends strongly on the wavelength and the medium adjacent to the metal film. Generally, approximately 50 nm thickness is best for measurements at a Ag/air interface in the visible wavelength regime. If the thickness differs too much from the optimum value, zero reflectivity can not be obtained. In detail, thinner films result in a broader and less pronounced minimum. Film thicknesses larger than the optimum value result in less distinct minima as well; however, the width does not increase significantly in this case.

Figure 4 shows the measured and simulated p-polarized reflectivity at the interface of a 49 nm thick silver film to air, obtained over a broad spectral range using three different OLEDs.

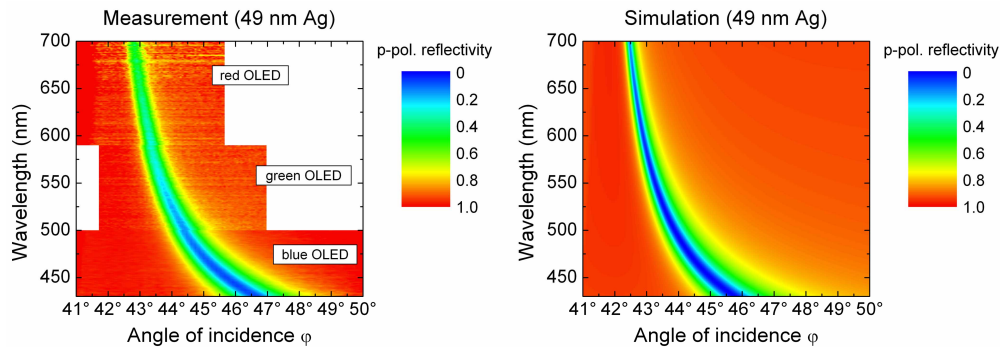


Fig. 4. Measurement (left) and simulation (right) of the spectral and angular resolved p-polarized reflectivity of a 49 nm thick silver film exposed to air. Regions of low reflectivity indicate resonant coupling to the surface plasmon.

The silver thickness was monitored with a quartz microbalance during the evaporation and subsequently controlled with profilometry (DekTak). The simulation was carried out with the commercial software ETFOS (Fluxim AG, Switzerland) using optical constants from ellipsometric measurements. At the chosen silver thickness it is expected that the resonance condition for the excitation of SPs is ideal and the reflectivity should drop to almost zero over a broad wavelength range as can be seen in the simulation. The observed angular dependence of the reflectivity minimum is in very good agreement with the simulation. Slight deviations of less than 1 degree in the angular position can be attributed to small errors in the optical constants used for the simulation. For wavelengths larger than 550 nm the full width at half maximum of the simulated reflectivity minimum is less than 0.5 degrees and can not be resolved anymore due to the finite angular resolution of the experimental setup. Therefore the measured intensity does not reach zero anymore. However, the angular position of the minimum still coincides well with the simulation.

In addition to the experiments at a Ag/air interface, we have performed measurements at a Au/air interface in order to illustrate the influence of the material that is used as sensing layer. The result for a gold film with a thickness of 49 nm is shown in Fig. 5. The overall agreement between experiment and simulation is again very good. The dispersion relation of the SPs has a smaller slope and is located at higher angles compared to silver. In addition, the SPR feature is much broader in the case of gold. For small wavelengths the SPR feature disappears completely and the reflectivity at the Au/air interface is low over the whole range of angles, because the frequency of light approaches the plasma frequency of gold. The optimum thickness for gold amounts to about 45 nm in the visible wavelength regime, but 49 nm still yield reasonable results and the minimum drops to almost zero.

The experiments performed at Ag/air and Au/air interfaces have demonstrated the basic functionality of the sensor. The good agreement between measured and simulated plasmon

dispersion relations allows predicting the angular position for a given wavelength also for media different than air, provided that the optical constants are known. This is advantageous for the measurements in aqueous environments shown in the following sections.

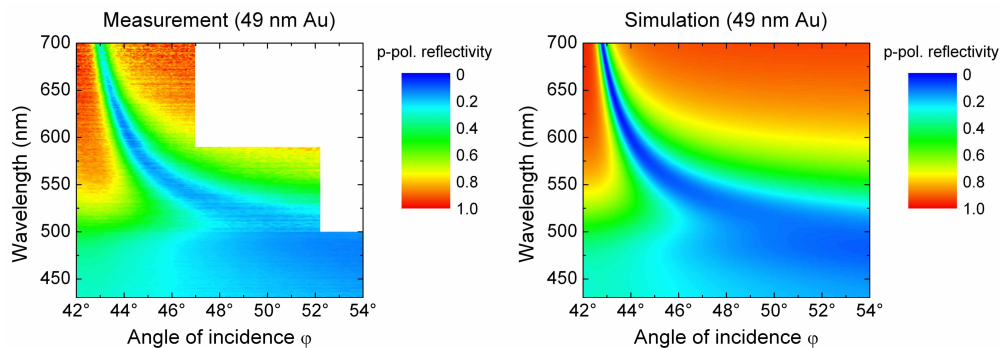


Fig. 5. Measurement (left) and simulation (right) of the spectral and angular resolved p-polarized reflectivity of a 49 nm thick gold film exposed to air.

### 3.2 Real time monitoring of temperature changes

To demonstrate the sensor's capability of performing measurements in real time, we monitored temperature changes and the dissolving process of NaCl in a water reservoir adjacent to the metallic sensing layer. For this purpose 48 nm Au were evaporated on an approximately 1 nm thick Ti undercoating layer to increase the adherence of gold on the glass substrate in contact with the aqueous environment. Gold is frequently used for sensing in aqueous environment because it is chemically more stable than silver. The red OLED was used as a light source in these experiments. Simulations predict that the SPR feature shifts to larger angles of about 70-80 degrees, if the Au layer is in contact with water. Thus, we have designed an optimized trapezoidal plexiglass prism so that the light from the OLED is incident on the metal film under an angle in that range. All experiments were performed at room temperature (20 °C) and the changes over time at a constant angle of incidence were monitored. By increasing the temperature of water it is expected that the spectral position of the minimum shifts to smaller wavelengths, because the refractive index of water is reduced with increasing temperature [18].

The measurement of the reflectivity as a function of wavelength at an incidence angle of approximately 74 degrees during the change of the water temperature is shown in Fig. 6. For the first five minutes the water reservoir next to the gold film was empty, thus we measured the reflectivity of a Au/air interface at an angle of incidence, which is far away from the resonant position. Therefore no minimum can be observed and the reflectivity of the gold film is very high over the whole wavelength range.

After five minutes we added pure water with a temperature of 25 °C. Instantly a pronounced SPR minimum appears with the lowest reflectivity at about 658 nm wavelength. The spectral position of the minimum remains constant until we start to heat and stir the water five minutes later. The increasing temperature causes the minimum to shift to lower wavelengths, which agrees with the expected behavior. After 40 minutes heating was stopped and the position of the minimum moves back to higher wavelengths as the water cools down.

For each time step a Gaussian fit to the reflectivity curve was carried out in order to obtain the spectral position of the minimum (red line in Fig. 6). We identify this position with the point of optimum excitation of SPs. The average position of the minimum in the first five minutes is used to define the value of  $n_{\text{Substrate}} \cdot \sin \varphi$  (see Eq. 2), as the angle of incidence is not known precisely. We find a value of 1.437 which is close to the value of 1.43 that is expected for  $\varphi = 74^\circ$  and  $n_{\text{Substrate}} = 1.49$  (plexiglass). Then the dielectric constant  $\epsilon_2$  of the

adjacent water reservoir can be determined using Eq. (2), and therewith the refractive index  $n_2 = \sqrt{\epsilon_2}$  for each time step can be calculated.

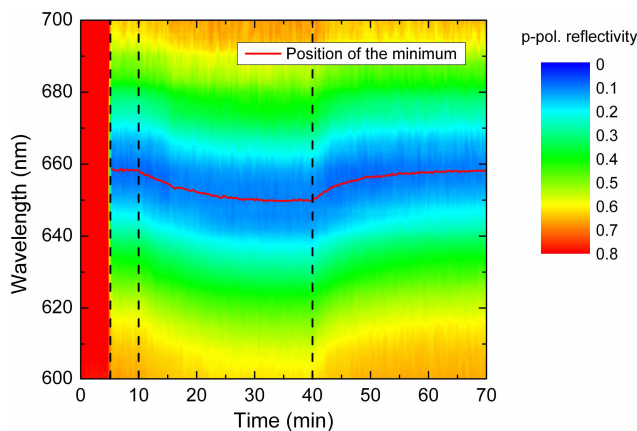


Fig. 6. Measurement of the reflectivity change over time of a 48 nm Au film adjacent to a water reservoir at an incidence angle of approximately 74 degrees. Initially, the cuvette is empty, hence we measure the reflectivity of a Au/air interface and no SPR feature is observable at this angle. After five minutes water with a temperature of 25 °C was added. Five minutes later we started to heat and stir the water. This induces a shift of the minimum to smaller wavelengths with increasing temperature. After 40 minutes heating was stopped. The water cools down and the minimum moves back to higher wavelengths again

Figure 7 shows the refractive index that was deduced from the spectral position of the minimum. Finally, the temperature of the water reservoir can be derived through the correlation between temperature and refractive index of water [18]. The result is also plotted in Fig. 7. The temperature reaches a maximum of about 57 °C. This value is about 10 °C lower than the temperature that was obtained with a comparative measurement using a temperature sensor (Pt100) placed directly inside the water reservoir. The difference may arise from the fact that the water temperature is not isotropic inside the reservoir and especially lower near the gold film because the contact to the prism acts as a heat sink.

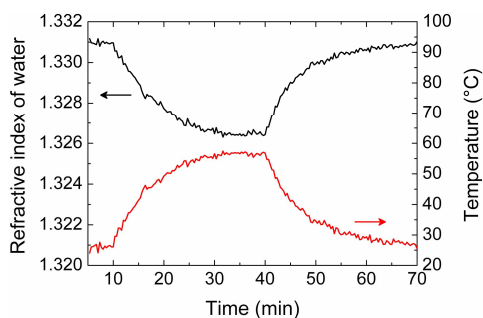


Fig. 7. Extracted refractive index and temperature of water from the spectral position of the minimum in Fig. 6.

### 3.3 Measurement of the dissolving process of sodium chloride

SPR sensors are widely used to monitor biospecific interactions or to determine concentrations of biomolecules in a solvent. To demonstrate the feasibility of our sensor to detect changes in concentration in real time, we have dissolved sodium chloride in a water reservoir adjacent to the same 48 nm gold film used in the previous experiment. It is expected

that the spectral position of the minimum shifts to higher wavelengths with increasing NaCl concentration [19]. Therefore it is reasonable to start at a larger incidence angle so that the initial position of the minimum is located at a lower wavelength compared to the previous experiment. Figure 8 shows the reflectivity of a Au/water interface as a function of wavelength and time at an incidence angle of approximately 76 degrees.

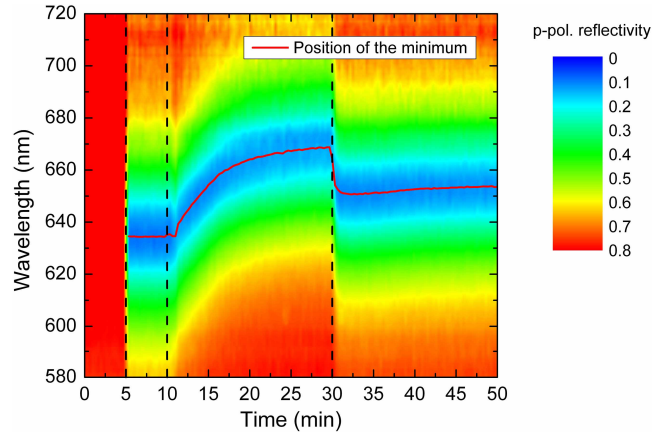


Fig. 8. Wavelength and time dependent reflectivity of a Au/water interface at an incidence angle of approximately 76 degrees. The water reservoir is empty in the beginning. After five minutes we added 4.5 ml water. Five minutes later we added 0.5 g NaCl. The salt slowly dissolves and the spectral position of the minimum shifts to higher wavelengths. After 30 minutes we added 5 ml water which causes a dilution and the minimum moves back to lower wavelengths.

Like in the measurement of the temperature change, the water reservoir was empty for the first five minutes. Again there is no SPR feature observable and the reflectivity is high over the entire wavelength range. After adding 4.5 ml of water, which is sufficient to cover the gold film completely with water, a pronounced minimum appears. The lowest reflectivity is located at a wavelength of about 634.5 nm since we measure at a higher incidence angle. After ten minutes 0.5 g of NaCl were added and after one more minute stirring of the water reservoir was started. The salt slowly dissolves and the minimum position shifts to higher wavelengths with increasing salt concentration. After 30 minutes we added another 5 ml of pure water. This dilution instantaneously reduces the concentration of NaCl and the minimum position moves back to lower wavelengths.

To obtain the refractive index of the solution from the spectral position of the SPR feature, a value of  $n = 1.3329$  for pure water was used for the position of the minimum between  $t = 5$  min and 10 min. For  $t > 10$  min the spectral position of the minimum was obtained similar to the previous experiment. The index of refraction was again calculated using Eq. (2) and is shown in Fig. 9. The increase of the refractive index with the concentration of dissolved sodium chloride  $c_{\text{NaCl}}$  (in wt.%) is well described by the following equation

$$n = 0.00177 c_{\text{NaCl}} + 1.3329, \quad (3)$$

which was derived from data in Ref. 19. Although this equation is strictly valid only for one specific wavelength ( $\lambda = 589$  nm), it is used in the whole wavelength range between 634 nm and 670 nm, as the change of the refractive index with wavelength is comparatively small. We used Eq. (3) to extract the concentration of sodium chloride in the solution as depicted in Fig. 9.

The maximum measured NaCl concentration is 10.8 wt.% and drops to 5.5 wt.% after the dilution. The theoretical concentration that is derived from the amount of inserted water and salt should be 10 wt.% before and 5 wt.% after the dilution, respectively. The difference

between the measurement and the expected value possibly results from the evaporation of water due to the stirring. This could also explain the slow increase over time after the dilution.

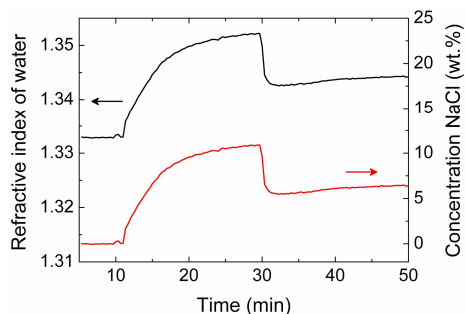


Fig. 9. Extracted refractive index of water and salt concentration from the spectral position of the minimum in Fig. 8.

This experiment demonstrates that the sensor is capable of monitoring the concentration of dissolved NaCl in water in real time, thus the sensor also has the potential of measuring concentrations of other materials or biomolecules within a solvent.

### 3.4 Discussion

The sensitivity of an SPR sensor is determined by the magnitude of the wavelength shift divided by the change in refractive index [20]. It is given in units of nanometers per refractive index units (nm/RIU), where the difference between a refractive index of 1.4 and 1.3 is equal to 0.1 RIU. For the measurements at Au/water interfaces, the wavelength shifts by approximately 16 nm if the refractive index changes by 0.01, thus the sensitivity is around 1600 nm/RIU. In general, the sensitivity is higher at smaller angles because the dispersion relation has a larger slope.

White and Fan emphasize that the sensor resolution, which characterizes the smallest possible spectral shift that can be accurately measured, is an equally important property of an SPR device [20]. In our setup the sensor resolution is approximately 1 nm. The detection limit, which is the ratio between sensor resolution and sensitivity, is then around  $6 \times 10^{-4}$  RIU. For the temperature measurement, this corresponds to a temperature change of approximately 5 K, which should be considered as a very conservative number, as Fig. 7 clearly shows the capability to monitor smaller temperature changes. The detection limit for the concentration of NaCl is about 0.3 wt.%. For the measurement of the concentration of biomolecules within a solvent the latter value could be greatly increased by using a functionalized gold surface.

The sensitivity could be enhanced by using silver instead of gold. Although the worse chemical stability of silver might generate problems in aqueous environments, a sensor comprising a silver film is ideally suited for measurements at silver/air interfaces, for instance as a gas sensor. Especially at small angles (equivalent to high wavelengths) the sensitivity can be close to the demonstrated sensitivity of prism coupled SPR sensors of 7120 nm/RIU [20].

In addition, the sensor resolution can be further increased by reducing the signal-to-noise ratio, for instance by operating the OLED at a higher brightness. The signal-to-noise ratio could be further optimized by decreasing the width of the SPR feature, for instance by utilizing optical multilayer-structures supporting symmetrically bound surface plasmons [21]. It should be noted that it is very important to choose the optimal metal thickness for the wavelength range under consideration so that the signal-to-noise ratio is maximal.

Furthermore, the usage of a white OLED could be favorable for covering a larger spectral range, hence making it possible to use the sensor in a wide range of applications. By contrast, a narrower emission spectrum might be advantageous for specific measurements in a small wavelength range. Due to the fact that the OLED has a spectrally extended emission it is not possible to achieve the same resolution and detection limit as a device with a laser light

source. However, we want to emphasize that in contrast to SPR devices based on a laser, our sensor offers the advantage that there is no necessity to couple light from external bulky sources into the device which makes the sensor particularly interesting for miniaturization and for low-cost applications.

#### **4. Conclusions**

We have demonstrated a novel SPR sensor based on the combination of a metallic sensing layer and an integrated OLED light source located on opposite sides of a prism. We have analyzed the spectral and angular dependent intensity of the reflected light for sensing layers consisting of silver and gold and we have shown the importance of choosing the appropriate metal thickness. The measurements at metal/air interfaces are in very good agreement with the simulations. Further on, we have demonstrated that the sensor is capable of real time monitoring temperature changes inside an adjacent water reservoir. In addition, we have recorded the dissolving process of sodium chloride in water in real time. This shows that the configuration could in principle also be used for bio-sensing applications like the label-free analysis of protein interactions or adsorption processes as well as for the determination of concentrations of a given material within a solvent.

We anticipate that the presented SPR configuration can be monolithically integrated on one common substrate, thus making it unnecessary to use a prism. It is also particularly compatible with the planar glass light pipe platform for SPR sensing, reported by several authors [1,22]. An additional benefit of the usage of an OLED is that the active area can easily be adjusted to any shape required for a specific application. Finally, we want to mention that our sensor can in principle be used for the simultaneous determination of the thickness and dielectric constant of thin films. Because it is impossible to obtain both of these parameters from a single SPR experiment, Peterlinz and Georgiadis have proposed to use two lasers with different wavelengths in one experiment to measure both thin film quantities at the same time [4]. Due to the broad emission range of OLEDs it should be possible to realize this idea with only one OLED. However, even a second OLED could be placed directly adjacent to the first OLED, thus offering for example a simultaneous red and blue emission without reducing the tremendous potential for miniaturization.

#### **Acknowledgments**

We acknowledge financial support by the Elite Network of Bavaria through the international graduate school “Materials Science of Complex Interfaces” as well as OSRAM OS for providing us with some of the OLED materials.